catalysts

MDPI

Article

Catalytic Activity Enhancement of Cu-Zn-Based Catalyst for Methanol Steam Reforming with Magnetic Inducement

Sasimas Katanyutanon, Dilpium Samarasinghe, Luckhana Lawtrakul * and Pisanu Toochinda *

School of Bio-Chemical Engineering and Technology, Sirindhorn International Institute of Technology, Thammasat University, P.O. Box 22, Pathumthani 12121, Thailand; por.katanyutanon@gmail.com (S.K.); dilpiumsamarasinghe@gmail.com (D.S.)

* Correspondence: luckhana@siit.tu.ac.th (L.L.); pisanu@siit.tu.ac.th (P.T.)

Abstract: Magnetic inducement was applied during metal loading to enhance Cu-Zn catalysts for methanol steam reforming in the temperature range of 200–300 °C. The supports used in this study were the γ-Al_2O_3 support and CeO_2-Al_2O_3 supports prepared under different magnetic environments. Cu-Zn loading between the north and south poles (N-S) on the CeO_2-Al_2O_3 support, prepared between two north poles (N-N), led to the highest H_2 production at 300 °C (2796 ± 76 µmol/min), which is triple that of Cu-Zn/CeO_2-Al_2O_3 prepared without magnetic inducement and ~11-fold the activity of the Cu-Zn/Al_2O_3 reference catalyst. The N-S magnetic environment during metal loading leads to lower reduction temperatures and larger Cu(1+):Cu(2+) ratio. These results showed that the pole arrangement of magnets during metal loading could affect the catalytic activity of the Cu-Zn catalyst owing to its influence on the reducibility and the oxidation state of Cu active metal.

Keywords: methanol steam reforming; Cu-Zn catalyst; magnetic inducement; Cu reducibility

Citation: Katanyutanon, S.; Samarasinghe, D.; Lawtrakul, L.; Toochinda, P. Catalytic Activity Enhancement of Cu-Zn-Based Catalyst for Methanol Steam Reforming with Magnetic Inducement. *Catalysts* **2021**, *11*, 1110. https://doi.org/10.3390/catal11091110

Academic Editor: Leonarda Francesca Liotta

Received: 23 August 2021
Accepted: 14 September 2021
Published: 16 September 2021

1. Introduction

Methanol steam reforming (MSR) is a promising reforming reaction of hydrocarbon for hydrogen production, as shown in Equation (1). MSR can be considered as sustainable because methanol can be obtained from renewable sources such as crops and agricultural waste [1–4].

$$CH_3OH + H_2O \rightleftharpoons 3H_2 + CO_2 \qquad H_{298} = +50\ kJ/mol \tag{1}$$

Noble metal catalysts, e.g., Pt, Pd, Ru, and Rh, are reported in the literature as stable, active catalysts for MSR; however, they are less suitable for commercial applications owing to the high price and low availability [5–7]. Cu-Zn-based catalyst is a non-noble catalyst that is widely studied and used for MSR due to its high selectivity toward H_2 and CO_2 [8–11]. Zn is commonly added to Cu-based catalysts to serve as an electron donor to Cu to promote its reducibility to the active forms for MSR, which are metallic Cu and Cu_2O [12–14]. For the electron transfer to happen, Cu and Zn must be located in close proximity; thus, good dispersion of both metals is required [15]. However, Cu-Zn-based catalysts suffer from deactivation by sintering at high temperatures (>300 °C) [16]. Improving the dispersion of Cu-Zn can also inhibit sintering at high temperatures [17].

The sol-gel catalyst preparation technique is commonly known to improve the distribution of active metals compared to other catalyst preparation methods [18,19]. Yet, the literature reports that CuO-ZnO-Al_2O_3 catalysts prepared via a sol-gel method showed an increased particle size and decreased metal dispersion with an increase in Cu and Zn contents, implying that the conventional sol-gel method can be modified to create better dispersion of active metals over the support [20]. Inducement with magnetic field has been applied in preparation of catalysts with ferromagnetic components such as Co and Ni to drive the deposition process and control the shape of nanoparticles or the long-range order in the crystal lattice [21–24]. There has not been any research on magnetic inducement

during metal loading on catalyst supports, especially for metals with paramagnetic and diamagnetic properties. The literature reported that paramagnetic and diamagnetic ions in a dilute solution move differently under the influence of an external magnetic field [25–27]. An application of an external magnetic field during CeO_2-Al_2O_3 support preparation has been previously studied in our lab. Magnetic inducement was found to affect the dispersion of CeO_2 in the Al_2O_3 framework and consequently cause improvements in the catalytic performance of Ni catalysts for ammonia decomposition and ethanol steam reforming [28,29].

In this work, the active metal loading process involves both the paramagnetic Cu^{2+} ion and Zn^{2+} diamagnetic ion. Magnetic inducement is applied during the loading of Cu-Zn active metal with the hypothesis that it will affect the activity and properties of the Cu-Zn catalysts. According to our previous study showing that CeO_2-Al_2O_3 supports prepared under magnetic inducement can affect steam reforming activity, CeO_2-Al_2O_3, as well as γ-Al_2O_3, was chosen as the catalyst supports in this study. The main objective of this study is to modify Cu-Zn-based catalyst on CeO_2-Al_2O_3 supports to improve the hydrogen production rate at low reaction temperatures (<300 °C) from MSR by the application of magnetic inducement during active metal loading via the sol-gel method.

2. Results

2.1. Effect of CeO_2-Al_2O_3 Supports Prepared under Magnetic Inducement on H_2 Production

The supports used in this study were CeO_2-Al_2O_3, prepared under magnetic inducement which has been found to increase the catalytic performance of Ni catalysts in a previous work [28,29]. To confirm whether they can also improve the activity of the Cu-Zn catalyst for MSR, a study was performed on Cu-Zn catalysts loaded without magnetic inducement on CeO_2-Al_2O_3 supports prepared under different magnetic environments, which are (1) under no magnetic field (no magnet), (2) between north–north magnetic poles (N-N), and (3) between north–south magnetic poles (N-S).

Table 1 shows hydrogen production rates from MSR using Cu-Zn catalysts supported on CeO_2-Al_2O_3 prepared with and without magnetic inducement between 200 and 300 °C. The results show that within this temperature range, the Cu-Zn catalyst loaded on the N-N support yields twice the hydrogen production of the catalyst loaded on the support prepared under no magnetic field. These results correspond with the activity results of Ni/CeO_2-Al_2O_3 catalysts reported in previous studies which found that the CeO_2-Al_2O_3 support prepared between N-N magnetic poles possesses the highest Ce composition and uniform Ce distribution in the Al_2O_3 framework [28,29].

Table 1. H_2 production rate of Cu-Zn catalysts (no magnet) on CeO_2-Al_2O_3 supports prepared with and without magnetic inducement. The magnetic environments are between north–north magnetic poles (N-N) and between north–south magnetic poles (N-S).

Magnetic Inducement	H_2 Production Rate (μmol/min)				
	200 °C	225 °C	250 °C	275 °C	300 °C
No magnet	150 ± 30	371 ± 43	619 ± 61	850 ± 80	1095 ± 81
N-N	175 ± 50	754 ± 60	1349 ± 99	1800 ± 97	2099 ± 98
N-S	167 ± 42	530 ± 40	916 ± 42	1388 ± 72	2002 ± 76

The supports in this study have also been characterized in the same way as in our previous work [29]. Table 2 lists the physical properties of γ-Al_2O_3 and CeO_2-Al_2O_3 supports including surface area, pore volume, and pore diameter determined by the N_2 physical adsorption calculated using the Brunauer, Emmett and Teller (BET) technique. From the results in Table 2, it can be observed that out of the CeO_2-Al_2O_3 supports, the support prepared under the N-N magnetic environment has the lowest surface area, which implies higher Ce composition in the Al_2O_3 framework, while in the same category, the CeO_2-Al_2O_3 support prepared under the N-S magnetic environment has the highest surface

area, which indicates a relatively low Ce composition in the support framework. These results correspond well with the lattice constants calculated using Scherrer's equation shown in Table S1. An analysis with scanning electron microscopy coupled with energy dispersive X-ray spectroscopy (SEM-EDS) was also carried out to determine the Ce:Al molar ratio in the supports, as shown in Figure S1 and Table S2. CeO_2-Al_2O_3 (N-N) shows a large average Ce:Al molar ratio with relatively small standard deviation. This confirms the speculation that magnetic inducement can cause a change in Ce dispersion in the support framework.

Table 2. Surface area, pore volume, and average pore diameter of γ-Al_2O_3 and CeO_2-Al_2O_3 supports with and without magnetic inducement, calculated using the Brunauer, Emmett and Teller technique.

Support	Magnetic Inducement	Surface Area (m^2/g)	Pore Volume (cm^3/g)	Average Pore Diameter (Å)
γ-Al_2O_3	No magnet	180.5	0.31	69.2
CeO_2	No magnet	46.6	0.11	80.0
CeO_2-Al_2O_3	No magnet	142.1	0.32	86.3
	N-N	134.2	0.31	84.6
	N-S	139.5	0.33	85.4

Since the properties of the supports are comparable to those reported in our previous study, it can be assumed that better dispersion of Ce in the support framework also helps with distribution of Cu atoms on the support surface. This assumption is supported by the literature which reported that uniformly dispersed Ce atoms in the Al_2O_3 framework might have helped to disperse Cu-Zn active metals over the support [30]. Due to these results, the rest of this study continued with this set of supports.

2.2. Effects of Magnetic Inducement during Cu-Zn Active Metal Loading

2.2.1. Hydrogen Production of Cu-Zn Catalysts Prepared with Magnetic Inducement during Metal Loading

The effects of magnetic inducement during Cu-Zn loading were studied on γ-Al_2O_3 reference support and CeO_2-Al_2O_3 supports prepared under different magnetic environments. Figure 1 shows the hydrogen production rates of Cu-Zn catalysts loaded with and without magnetic inducement on three supports, which are γ-Al_2O_3, CeO_2-Al_2O_3 (no magnet), and CeO_2-Al_2O_3 (N-N). The results from Cu-Zn catalysts on the CeO_2-Al_2O_3 (N-S) support were omitted to avoid overcrowding the figure. They can be found together with the results from other supports in Tables S3–S6 in Supplementary Materials.

Figure 1 shows that catalysts loaded on CeO_2-Al_2O_3 supports yield H_2 production rates that are higher than catalysts loaded on γ-Al_2O_3 support. This might happen because partial doping of Ce into Al_2O_3 framework enhances the dispersion of Cu-Zn active metals [31]. Applying an N-N magnetic environment during CeO_2-Al_2O_3 support preparation leads to a higher composition and more uniform distribution of Ce in the Al_2O_3 framework compared to the non-magnetic situation, as shown in Table S3 and in our previous works [28,29]. These, in turn, enhance the Cu-Zn dispersion on the support, leading to H_2 production rates which are triple those from the catalysts loaded on CeO_2-Al_2O_3 (no magnet) support and ~8-fold of those from the catalysts loaded on γ-Al_2O_3 support on average. When considering different magnetic environments during Cu-Zn loading on a specific support, the catalysts loaded between N-S magnets provide a H_2 production rate which is double the yield given by the catalysts loaded under no magnetic environment.

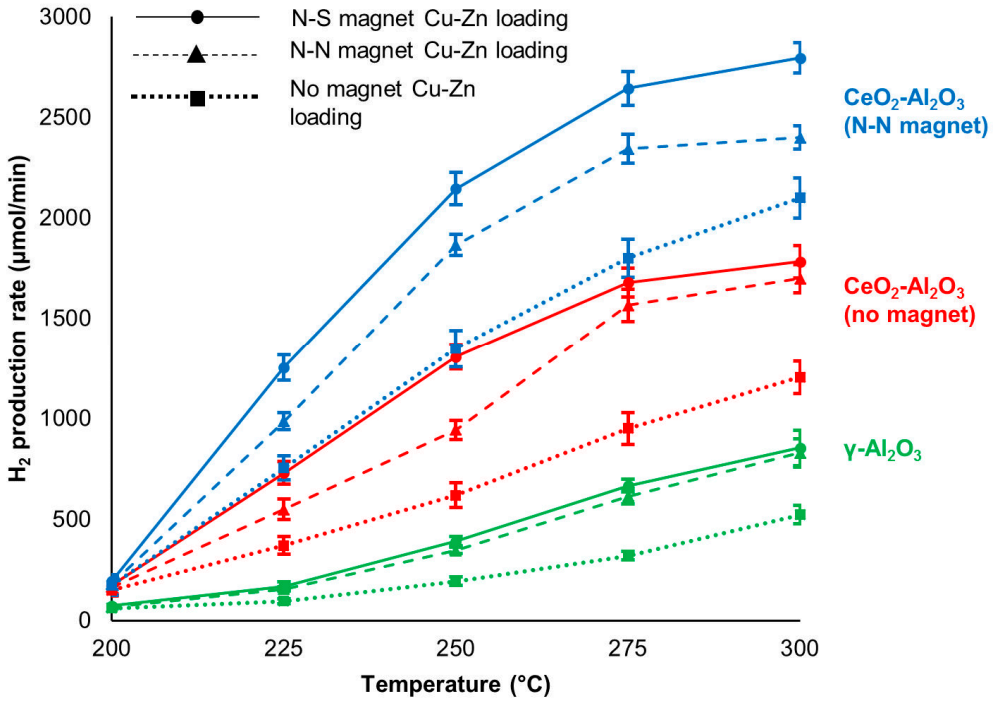

Figure 1. H_2 production rates of Cu-Zn catalysts on γ-Al_2O_3, CeO_2-Al_2O_3 (no magnet), and CeO_2-Al_2O_3 (N-N) supports.

Among the prepared catalysts, the Cu-Zn (N-S)/CeO_2-Al_2O_3 (N-N) catalyst shows the highest hydrogen yield in the 200–300 °C temperature range, agreeing with our earlier observation that the CeO_2-Al_2O_3 support prepared between N-N magnets is the best support in terms of hydrogen production rate. This result shows that magnetic inducement during metal loading can be utilized in combination with magnetic inducement during support preparation to further improve the catalytic activity.

To ensure that these effects were not due to variation in Cu and Zn contents, inductively coupled plasma–optical emission spectrometry (ICP-OES) analysis was performed on all the prepared catalysts. The Cu and Zn contents in all of the catalysts were 22.01 ± 0.45 and 21.09 ± 0.81 mg/g, respectively. These results correspond well with the intended Cu and Zn contents, which are 2.5% each. The deviations in Cu and Zn contents are not large enough to be considered as a main cause to the improved catalytic activity.

2.2.2. Temperature-Programmed Reduction (TPR) Profiles of Catalysts Prepared under Magnetic Inducement

To find out how magnetic inducement during Cu-Zn loading could affect the catalytic activity, the reducibility of Cu active metal on the catalysts was investigated. TPR analysis was performed on Cu-Zn catalysts loaded under different magnetic environments on CeO_2-Al_2O_3 (no magnet). The TPR profiles are presented in Figure 2. The reduction temperature corresponds to the energy required to reduce Cu^{2+}, which depends on the localization of Cu and Zn atoms on the support. Agglomeration of Cu clusters and Zn clusters will retard the electron mobility between Cu and Zn and decrease the reducibility of Cu^{2+}.

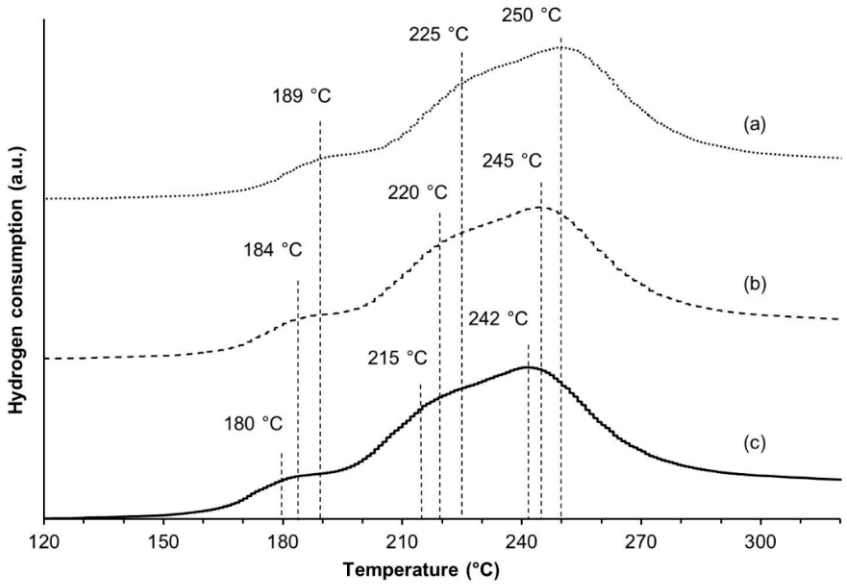

Figure 2. Temperature-programmed reduction profiles of (**a**) Cu-Zn (no magnet)/CeO_2-Al_2O_3 (no magnet), (**b**) Cu-Zn (N-N)/CeO_2-Al_2O_3 (no magnet), and (**c**) Cu-Zn (N-S)/CeO_2-Al_2O_3 (no magnet).

TPR profiles of all three catalysts in Figure 2 are similar, possessing three characteristic peaks: a high-intensity peak at ~250 °C, a shoulder peak at ~220 °C and a well-defined shoulder peak at ~180 °C. According to similar TPR profiles observed on Cu-CeO_2 and Cu/Zn-CeO_2 catalysts in the literature [32–36], the shoulder peaks at ~180 °C could be assigned to the reduction of small, non-crystalline CuO clusters which strongly interact with the CeO_2 surface, while the shoulder peaks at ~220 °C could come from larger CuO clusters with weaker interactions with CeO_2. The peaks at ~250 °C could be attributed to the reduction of bulk CuO in crystalline form with minimal association with CeO_2.

There is a difference in the reduction temperatures of these catalysts. The catalyst of which active metals were loaded under N-S magnetic inducement shows the lowest reduction temperature, implying that Cu^{2+} in this catalyst requires the least energy to reduce. The catalyst prepared with no magnetic field during metal loading exhibits the highest reduction temperature, implying that the reduction of Cu^{2+} is more difficult. Since the active forms of Cu for MSR are metallic Cu and Cu^{+}, this in turn reduces the hydrogen production. This result corresponds with the hydrogen production results obtained on Cu-Zn catalysts prepared with and without magnetic inducement on CeO_2-Al_2O_3 (no magnet) support, which are displayed in red in Figure 1.

2.2.3. X-ray Photoelectron Spectroscopy (XPS) Spectra of Catalysts Loaded under Magnetic Inducement

To investigate the influence of magnetic inducement on the oxidation states of Cu and Zn on the catalysts, XPS analysis was performed on Cu-Zn (no magnet)/CeO_2-Al_2O_3 (no magnet) and Cu-Zn (N-S)/CeO_2-Al_2O_3 (N-N). These catalysts were chosen to illustrate a clear change in Cu oxidation state because they exhibited the worst and the best H_2 production rates among the catalysts supported on CeO_2-Al_2O_3, respectively.

Figure 3 shows the Zn 2p XPS spectra of the catalysts. The Zn 2p 3/2 and Zn 2p 1/2 binding energies in both catalysts are 1021 and 1044 eV, respectively. No evident peak shift was observed, implying that magnetic inducement has a negligible effect on the oxidation state of Zn on the catalysts.

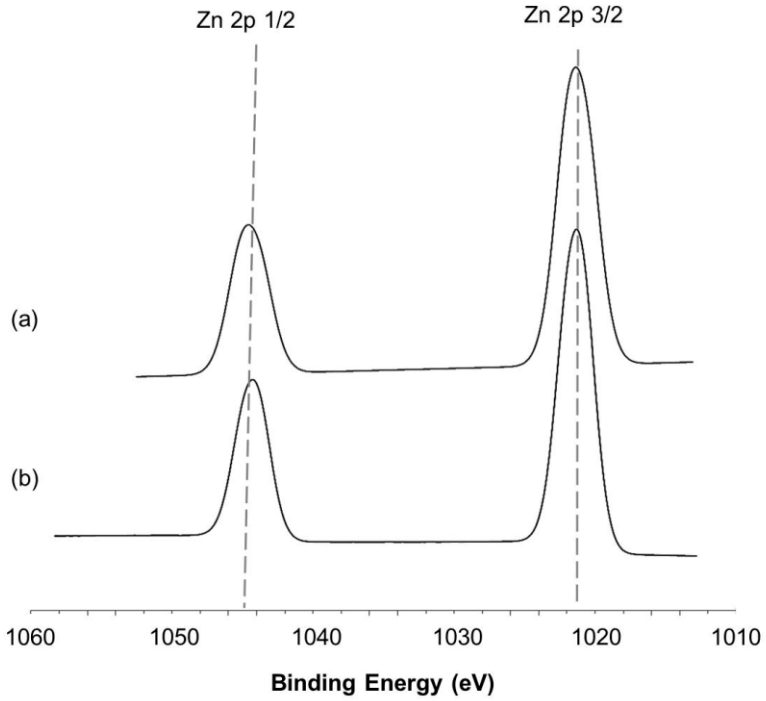

Figure 3. Zn 2p X-ray photoelectron spectroscopy (XPS) spectra of (**a**) Cu-Zn (no magnet)/CeO_2-Al_2O_3 (no magnet) and (**b**) Cu-Zn (N-S)/CeO_2-Al_2O_3 (N-N).

Figure 4 shows Cu 2p 3/2 XPS spectra of the catalysts. The peaks were deconvoluted to show the relative intensity of Cu(0), Cu(1+), and Cu(2+) peaks. However, the difference between the binding energies of Cu 2p (0) 3/2 and Cu 2p (1+) 3/2 main peaks is small. Auger spectroscopy would be required for a proper peak assignment in this region. The comparison in this study will, therefore, utilize the satellite peaks of Cu 2p 3/2 in 940–945 eV binding energy region. The areas of Cu 2p (1+) and Cu 2p (2+) satellite peaks and their ratios are shown in Table 3.

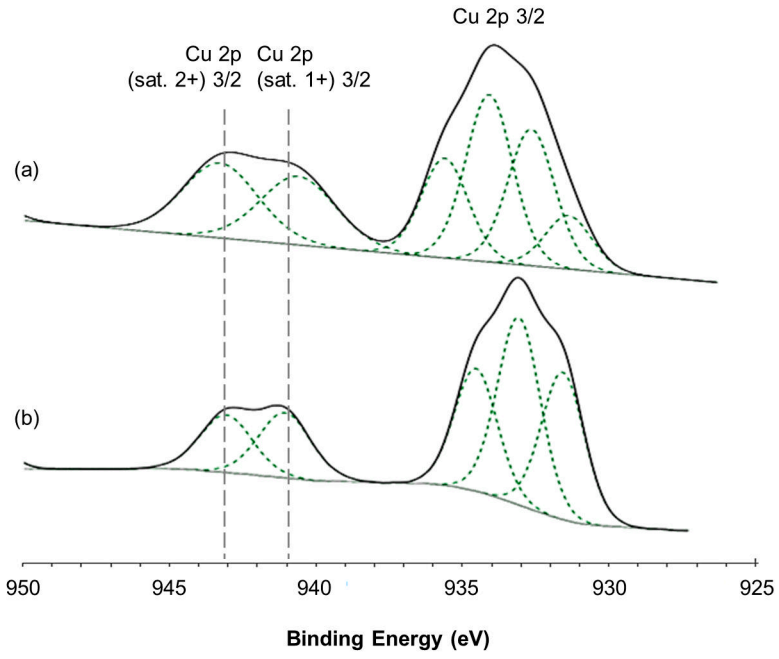

Figure 4. Cu 2p 3/2 XPS spectra with peak fittings of (**a**) Cu-Zn (no magnet)/CeO_2-Al_2O_3 (no magnet) and (**b**) Cu-Zn (N-S)/CeO_2-Al_2O_3 (N-N).

Table 3. Peak areas and area ratio of the satellite peaks of Cu 2p (1+) 3/2 and Cu 2p (2+) 3/2 determined by XPS.

Catalysts	Peak Area (%)		Area Ratio Cu(1+):Cu(2+)
	Cu (sat. 1+)	Cu (sat. 2+)	
Cu-Zn (no magnet) /CeO_2-Al_2O_3 (no magnet)	10.68	11.67	0.92
Cu-Zn (N-S) /CeO_2-Al_2O_3 (N-N)	8.69	7.67	1.13

From Table 3, the Cu(1+):Cu(2+) ratio is higher in the Cu-Zn (N-S)/CeO_2-Al_2O_3 (N-N) catalyst, which exhibits the highest H_2 production rate. The ratio of Cu(1+):Cu(2+) for Cu-Zn (no magnet)/CeO_2-Al_2O_3 (no magnet) is ~20% lower than that of the optimal catalyst. The high Cu(1+):Cu(2+) ratio in Cu-Zn (N-S)/CeO_2-Al_2O_3 (N-N) corresponds with other speculations that Cu^+ is an active form of Cu for MSR [12–14]. The higher ratio of Cu^+ in the optimal catalyst can be due to the better interaction between Cu and CeO_2 clusters that are dispersed in Al_2O_3 support framework or better electron transfer between Cu and Zn clusters that are located in close proximity.

3. Discussion

From the first part of this study, it is found that CeO_2-Al_2O_3 supports prepared in different magnetic environments can affect the activity of Cu-Zn catalysts, which is in line with the results from our previous studies on Ni catalysts. The best magnetic environment for support preparation is between two north poles. It is expected that the activity improvement stems from improved Ce dispersion in the support, which helps with Cu dispersion on the support. Magnetic inducement during metal loading also shows a positive effect on catalytic activity for MSR, of which the optimal magnetic environment is between the north and south poles. Therefore, the catalyst with the highest H_2 production rate in this study is Cu-Zn (N-S)/CeO_2-Al_2O_3 (N-N).

From TPR and XPS analyses, magnetic inducement during Cu-Zn metal loading seems to have an effect on the reducibility and the oxidation state of Cu. A magnetic environment during metal loading may provide an external driving force for both Cu^{2+} and Zn^{2+} ions to distribute on CeO_2-Al_2O_3 support, which results in a higher probability of Cu and Zn atoms being located in close proximity. Cu and Zn in proximity would allow Zn to serve as an electron donor to create a larger number of Cu^+ on the catalysts. This speculation may be able to explain the decrease in reduction temperature and the increase in Cu(1+):Cu(2+) ratio when comparing the Cu-Zn (N-S)/CeO_2-Al_2O_3 (N-N) catalyst to other catalysts. To verify this speculation, further characterization should be carried out on the local structure and interactions on the support.

4. Materials and Methods

4.1. Preparation of γ-Al_2O_3 Support

γ-Al_2O_3 support was prepared using sol-gel method. $Al(NO_3)_3 \cdot 9H_2O$ (≥98%, LOBA Chemie, Mumbai, India) was dissolved in deionized water to form a 1 M salt solution. Ammonia solution was added drop by drop to the Al salt solution to form gel until a pH of 9 was reached, within 90 min. The prepared gel was dried at 60 °C for 48 h, dried at 110 °C for 12 h, and calcined at 800 °C for 4 h. The support was ground and sieved at 106 μm.

4.2. Preparation of CeO_2-Al_2O_3 Supports under Magnetic Inducement

The preparation of CeO_2-Al_2O_3 supports with 5 mol% Ce content was carried out using the same sol-gel method as described above. Then, 0.5 M solutions of $Ce(NO_3)_3 \cdot 6H_2O$ (≥99%, Fluka, Seelze, Germany) and $Al(NO_3)_3 \cdot 9H_2O$ (≥98%, LOBA Chemie, Mumbai, India) were separately prepared by dissolving in deionized water. Both solutions were then mixed to form Ce-Al salt solutions with a 0.05:0.95 molar ratio. The Ce-Al salt solutions

were placed in different magnetic environments: under no magnetic field (no magnet), between north and south poles (N-S), and between two north poles (N-N). The setup of the magnetic field has been described elsewhere [28]. The details and scheme of the setup can also be found in Figure S2. The drying and calcination steps were carried out with the same steps as in γ-Al_2O_3 support preparation.

4.3. Cu-Zn Metal Loading under Magnetic Inducement on γ-Al_2O_3 and CeO_2-Al_2O_3 Supports

The preparation of Cu-Zn/γ-Al_2O_3 and Cu-Zn/CeO_2-Al_2O_3 catalysts with 5 wt% Cu-Zn metal loading was also carried out using sol-gel method. $Cu(NO_3)_2{\cdot}3H_2O$ (Sigma-Aldrich, St. Louis, MO, USA), $Zn(NO_3)_2{\cdot}6H_2O$ (Sigma-Aldrich, St. Louis, MO, USA), and citric acid monohydrate ($C_6H_8O_7{\cdot}6H_2O$, Merck, Burlington, MA, USA) were dissolved together in deionized water before the support was added. pH of the mixture was adjusted by slowly adding ammonia solution until it reached 7. The sol-gel catalysts were kept under different magnetic environments while drying at room temperature. The setup of the magnetic field was similar to the one used for support preparation shown in Figure S2, but the distance between the magnets was adjusted to 11 cm, and the number of magnets used on each side was reduced to one. The studied magnetic environments are no magnetic field (no magnet), between north and south poles (N-S), and between two north poles (N-N). After these samples became dry to touch, they were further dried at 110 °C for 16 h and calcined at 300 °C for 3 h. The calcined catalysts were then ground into a fine powder.

4.4. Catalytic Activity Testing for H_2 Production from MSR

The catalytic activity experiments were conducted using a quartz reactor with an inner diameter of 1 cm to determine gas production compositions from MSR. The catalyst (0.1 g) was mixed with quartz powder (0.4 g, Sigma-Aldrich, St. Louis, MO, USA) to reduce the temperature gradients inside the bed and packed between quartz wool to prevent the movement of the bed. The catalyst was reduced using 50 vol% H_2 (99.99% purity, Linde Thailand Pub Co., Ltd., Samut Prakan, Thailand) balanced in Ar (99.999% purity, Linde Thailand Pub Co., Ltd., Samut Prakan, Thailand) at 300 °C for 1 h with a total flow rate of 50 mL/min. The reactor was then purged with 20 mL/min of Ar at 300 °C for 15 min to remove excess H_2. Ar carrier gas at the flow rates of 20 mL/min flowed into saturators containing water at 100 °C and methanol at 65 °C, respectively. The feed reactant was a mixture of methanol and water with a molar ratio of 1:1. The catalyst activity tests were performed in a continuous mode at 200, 225, 250, 275 and 300 °C. The product gas was directly sent to the gas chromatography with a thermal conductivity detector (GCMS-2010 Ultra, Shimadzu Corporation, Kyoto, Japan) to determine the composition of the gaseous products. The catalytic activity testing was performed on 3 batches of catalysts and repeated 3 times for each catalyst. Stability test was also performed on Cu-Zn (N-S)/CeO_2-Al_2O_3 (N-N) and Cu-Zn (no magnet)/CeO_2-Al_2O_3 (no magnet) catalysts at 300 °C for 24 h continuously. The results from these stability tests can be found in Figures S3 and S4.

4.5. Support and Catalyst Characterization

Temperature-programmed reduction using 5 vol% H_2 in Ar (Linde Thailand Pub Co., Ltd., Samut Prakan, Thailand) was performed using a chemisorption analyzer (BELCAT-B, BEL Japan Inc., Osaka, Japan) to determine the effect of magnetic inducement on reduction temperature. Before each measurement, the samples were pre-treated in Ar at 300 °C for 30 min before cooling down to 30 °C. Temperature-programmed reduction was subsequently performed with 30 mL/min flow of 5 vol% H_2 in Ar, while the temperature increased from 30 to 350 °C at a rate of 10 °C/min and was then held at 350 °C for 30 min.

Conservation of Cu and Zn during metal loading was confirmed with ICP-OES (Optima 8300, PerkinElmer, Singapore) on microwave-digested catalysts. Microwave digestion of the catalysts was conducted in a mixture of 7 mL HCl and 3 mL HNO_3 at 190 °C for 1 h (Titan MPS, PerkinElmer, Rodgau, Germany) and filtered with grade 1 filter paper. The solution was then diluted to 100 mL in Type 1 deionized water.

The oxidation states of Cu and Zn were analyzed with XPS (Axis Supra, Kratos Analytical Ltd., Manchester, UK) using a monochromated Al Kα X-ray source operated at 450 mA and 15 kV. The Cu 2p spectra were deconvoluted using a Gaussian–Lorentzian mix of 0.3.

5. Conclusions

In this study, the catalytic activity of Cu-Zn catalyst for MSR was enhanced by introducing magnetic inducement during Cu-Zn loading and using CeO_2-Al_2O_3 support prepared with magnetic inducement. Application of a magnetic field during metal loading and support preparation affects the catalytic activity for MSR. Among all the catalysts in this study, Cu-Zn (N-S)/CeO_2-Al_2O_3 (N-N) exhibited the highest H_2 production of 2796 ± 76 µmol/min at 300 °C. This improvement in catalytic activity is ~3-fold when compared to Cu-Zn (no magnet)/CeO_2-Al_2O_3 (no magnet) and ~11-fold when compared to Cu-Zn (no magnet)/Al_2O_3 reference catalyst. From the XPS results, the Cu(1+):Cu(2+) ratio was determined. The Cu(1+):Cu(2+) ratio of Cu-Zn (N-S)/CeO_2-Al_2O_3 (N-N) was 1.13 compared to the ratio of 0.92 from Cu-Zn (no magnet)/CeO_2-Al_2O_3 (no magnet). Therefore, the 3-fold improvement in catalytic activity between Cu-Zn (N-S)/CeO_2-Al_2O_3 (N-N) and its non-magnetic-induced counterpart can be explained by higher Cu reducibility and the higher Cu(1+):Cu(2+) ratio. Therefore, the application of magnetic inducement is a novel technique for enhancing the catalytic activity of the Cu-Zn catalyst for MSR at low temperatures.

Supplementary Materials: The following are available online at https://www.mdpi.com/article/10.3390/catal11091110/s1, Table S1: Lattice constants of γ-Al_2O_3 and CeO_2-doped Al_2O_3 supports with and without magnetic inducement, Figure S1: SEM-EDS images of CeO_2-doped Al_2O_3 supports with and without magnetic inducement. (a) CeO_2-doped Al_2O_3 (no mag), (b) CeO_2-doped Al_2O_3 (N-S), (C) CeO_2-doped Al_2O_3 (N-N). The considered 5 points are circled in each support, Table S2: Ce distribution in CeO_2-doped Al_2O_3 supports with and without magnetic inducement, Table S3: H_2 production rate over Cu-Zn/γ-Al_2O_3 catalysts loaded with and without magnetic inducement, Table S4: H_2 production rate of Cu-Zn catalyst prepared over CeO_2-doped Al_2O_3 (no magnet) support. Cu-Zn metal loading was carried out with and without magnetic inducement, Table S5: H_2 production rate of Cu-Zn catalyst prepared over CeO_2-doped Al_2O_3 (N-S) support. Cu-Zn metal loading was carried out with and without magnetic inducement, Table S6: H_2 production rate of Cu-Zn catalyst prepared over CeO_2-doped Al_2O_3 (N-N) support. Cu-Zn metal loading was carried out with and without magnetic inducement, Figure S2: Magnet setup for support preparation, Figure S3: Stability test of Cu-Zn (N-S)/CeO_2-Al_2O_3 (N-N) at 300 °C for 24 h, Figure S4: Stability test of Cu-Zn (no magnet)/CeO_2-Al_2O_3 (no magnet) at 300 °C for 24 h.

Author Contributions: Conceptualization, P.T.; data curation, S.K. and D.S.; funding acquisition, P.T.; investigation, S.K., L.L. and P.T.; methodology, S.K. and D.S.; project administration, L.L. and P.T.; supervision, L.L. and P.T.; writing—original draft, S.K., D.S., L.L. and P.T.; writing—review and editing, L.L. and P.T. All authors have read and agreed to the published version of the manuscript.

Funding: This research was funded by Thammasat University Research Fund (TUFT 067/2563) and the thesis support from the Scholarship for Excellent Foreign Student, Sirindhorn International Institute of Technology, Thammasat University.

Conflicts of Interest: The authors declare no conflict of interest.

References

1. Sá, S.; Silva, H.; Brandão, L.; Sousa, J.M.; Mendes, A. Catalysts for methanol steam reforming—A review. *Appl. Catal. B Environ.* **2010**, *99*, 43–57. [CrossRef]
2. Pérez-Hernández, R.; Mendoza-Anaya, D.; Gutiérrez Martínez, A.; Gómez-Cortés, A. Catalytic Steam Reforming of Methanol to Produce Hydrogen on Supported Metal Catalysts. In *Hydrogen Energy—Challenges and Perspectives*; Minić, D., Ed.; IntechOpen: London, UK, 2012; pp. 149–174, ISBN 978-953-51-4271-3.
3. Madej-Lachowska, M.; Kulawska, M.; Słoczyński, J. Methanol as a high purity hydrogen source for fuel cells: A brief review of catalysts and rate expressions. *Chem. Process Eng.* **2017**, *38*, 147–162. [CrossRef]

4. Palo, D.R.; Dagle, R.A.; Holladay, J.D. Methanol Steam Reforming for Hydrogen Production. *Chem. Rev.* **2007**, *107*, 3992–4021. [CrossRef]
5. Papavasiliou, J.; Paxinou, A.; Słowik, G.; Neophytides, S.; Avgouropoulos, G. Steam Reforming of Methanol over Nanostructured Pt/TiO_2 and Pt/CeO_2 Catalysts for Fuel Cell Applications. *Catalysts* **2018**, *8*, 544. [CrossRef]
6. Tahay, P.; Khani, Y.; Jabari, M.; Bahadoran, F.; Safari, N. Highly porous monolith/TiO_2 supported Cu, Cu-Ni, Ru, and Pt catalysts in methanol steam reforming process for H_2 generation. *Appl. Catal. A Gen.* **2018**, *554*, 44–53. [CrossRef]
7. Rameshan, C.; Stadlmayr, W.; Penner, S.; Lorenz, H.; Memmel, N.; Hävecker, M.; Blume, R.; Teschner, D.; Rocha, T.; Zemlyanov, D.; et al. Hydrogen Production by Methanol Steam Reforming on Copper Boosted by Zinc-Assisted Water Activation. *Angew. Chem. Int. Ed. Engl.* **2012**, *51*, 3002–3006. [CrossRef]
8. Mrad, M.; Gennequin, C.; Aboukaïs, A.; Abi-Aad, E. Cu/Zn-based catalysts for H_2 production via steam reforming of methanol. *Catal. Today* **2011**, *176*, 88–92. [CrossRef]
9. Lindström, B.; Pettersson, L.J.; Menon, P.G. Activity and characterization of Cu/Zn, Cu/Cr and Cu/Zr on γ-alumina for methanol reforming for fuel cell vehicles. *Appl. Catal. A Gen.* **2002**, *234*, 111–125. [CrossRef]
10. Turco, M.; Bagnasco, G.; Costantino, U.; Marmottini, F.; Montanari, T.; Ramis, G.; Busca, G. Production of hydrogen from oxidative steam reforming of methanol I. Preparation and characterization of $Cu/ZnO/Al_2O_3$ catalysts from a hydrotalcite-like LDH precursor. *J. Catal.* **2004**, *228*, 43–55. [CrossRef]
11. Shishido, T.; Yamamoto, Y.; Morioka, H.; Takaki, K.; Takehira, K. Active Cu/ZnO and $Cu/ZnO/Al_2O_3$ catalysts prepared by homogeneous precipitation method in steam reforming of methanol. *Appl. Catal. A Gen.* **2004**, *263*, 249–253. [CrossRef]
12. Mrad, M.; Hammoud, D.; Gennequin, C.; Aboukaïs, A.; Abi-Aad, E. A comparative study on the effect of Zn addition to Cu/Ce and Cu/Ce-Al catalysts in the steam reforming of methanol. *Appl. Catal. A Gen.* **2014**, *471*, 84–90. [CrossRef]
13. Chiu, K.L.; Kwong, F.L.; Ng, D.H.L. Oxidation states of Cu in the $CuO/CeO_2/Al_2O_3$ catalyst in the methanol steam reforming process. *Curr. Appl. Phys.* **2012**, *12*, 1195–1198. [CrossRef]
14. Oguchi, H.; Kanai, H.; Utani, K.; Matsumura, Y.; Imamura, S. Cu_2O as active species in the steam reforming of methanol by CuO/ZrO_2 catalysts. *Appl. Catal. A Gen.* **2005**, *293*, 64–70. [CrossRef]
15. Kurr, P.; Kasatkin, I.; Girgsdies, F.; Trunschke, A.; Schlögl, R.; Ressler, T. Microstructural characterization of $Cu/ZnO/Al_2O_3$ catalysts for methanol steam reforming—A comparative study. *Appl. Catal. A Gen.* **2008**, *348*, 153–164. [CrossRef]
16. Zhang, R.; Huang, C.; Zong, L.; Lu, K.; Wang, X.; Cai, J. Hydrogen Production from Methanol Steam Reforming over TiO_2 and CeO_2 Pillared Clay Supported Au Catalysts. *Appl. Sci.* **2018**, *8*, 176. [CrossRef]
17. Yao, C.Z.; Wang, L.C.; Liu, Y.M.; Wu, G.S.; Cao, Y.; Dai, W.L.; He, H.Y.; Fan, K.N. Effect of preparation method on the hydrogen production from methanol steam reforming over binary Cu/ZrO_2 catalysts. *Appl. Catal. A Gen.* **2006**, *297*, 151–158. [CrossRef]
18. Yao, D.; Yang, H.; Chen, H.; Williams, P.T. Co-precipitation, impregnation and so-gel preparation of Ni catalysts for pyrolysis-catalytic steam reforming of waste plastics. *Appl. Catal. B Environ.* **2018**, *239*, 565–577. [CrossRef]
19. Sharifi, M.; Haghighi, M.; Rahmani, F.; Karimipour, S. Syngas production via dry reforming of CH_4 over Co- and Cu-promoted Ni/Al_2O_3-ZrO_2 nanocatalysts synthesized via sequential impregnation and sol-gel methods. *J. Nat. Gas Sci. Eng.* **2014**, *21*, 993–1004. [CrossRef]
20. Fornari, A.C.; Menechini Neto, R.; Lenzi, G.G.; dos Santos, O.A.A.; de Matos Jorge, L.M. Utilization of sol-gel CuO-ZnO-Al_2O_3 catalysts in the methanol steam reforming for hydrogen production. *Can. J. Chem. Eng.* **2017**, *95*, 2258–2271. [CrossRef]
21. Li, H.; Liao, J.; Du, Y.; You, T.; Liao, W.; Wena, L. Magnetic-field-induced deposition to fabricate multifunctional nanostructured Co, Ni, and CoNi alloy films as catalysts, ferromagnetic and superhydrophobic materials. *Chem. Commun.* **2013**, *49*, 1768–1770. [CrossRef] [PubMed]
22. Yang, Z.; Wei, J.; Bonville, P.; Pileni, M.P. Engineering the Magnetic Dipolar Interactions in 3D Binary Supracrystals Via Mesoscale Alloying. *Adv. Funct. Mater.* **2015**, *25*, 4908–4915. [CrossRef]
23. Lalatonne, Y.; Motte, L.; Russier, V.; Ngo, A.T.; Bonville, P.; Pileni, M.P. Mesoscopic Structures of Nanocrystals: Collective Magnetic Properties Due to the Alignment of Nanocrystals. *J. Phys. Chem. B* **2004**, *108*, 1848–1854. [CrossRef]
24. Yang, Z.; Wei, J.; Bonville, P.; Pileni, M.P. Beyond Entropy: Magnetic Forces Induce Formation of Quasicrystalline Structure in Binary Nanocrystal Superlattices. *J. Am. Chem. Soc.* **2015**, *137*, 4487–4493. [CrossRef] [PubMed]
25. Fujiwara, M.; Chie, K.; Sawai, J.; Shimizu, D.; Tanimoto, Y. On the Movement of Paramagnetic Ions in an Inhomogeneous Magnetic Field. *J. Phys. Chem. B* **2004**, *108*, 3531–3534. [CrossRef]
26. Fujiwara, M.; Mitsuda, K.; Tanimoto, Y. Movement and Diffusion of Paramagnetic Ions in a Magnetic Field. *J. Phys. Chem. B* **2006**, *110*, 13965–13969. [CrossRef] [PubMed]
27. Zhu, G.-P.; Hejiazan, M.; Huang, X.; Nguyen, N.-T. Magnetophoresis of diamagnetic microparticles in a weak magnetic field. *Lab Chip* **2014**, *14*, 4609–4615. [CrossRef] [PubMed]
28. Vacharapong, P.; Arayawate, S.; Henpraserttae, S.; Katanyutanon, S.; Charojrochkul, S.; Lawtrakul, L.; Toochinda, P. Effect of Magnetic Inducement in Preparation of Ni/Ce-doped Al_2O_3 for Ammonia Decomposition. *ChemistrySelect* **2019**, *4*, 11913–11919. [CrossRef]
29. Vacharapong, P.; Arayawate, S.; Katanyutanon, S.; Toochinda, P.; Lawtrakul, L.; Charojrochkul, S. Enhancement of Ni Catalyst Using CeO_2–Al_2O_3 Support Prepared with Magnetic Inducement for ESR. *Catalysts* **2020**, *10*, 1357. [CrossRef]
30. Mrad, M.; Gennequin, C.; Aboukaïs, A.; Abi-Aad, E. The performance of the Cu-Zn/CeO_2 catalysts in the steam reforming of methanol reaction. *Adv. Mater. Res.* **2011**, *324*, 157–161. [CrossRef]

31. Liu, Y.; Hayakawa, T.; Tsunoda, T.; Suzuki, K.; Hamakawa, S.; Murata, K.; Shiozaki, R.; Ishii, T.; Kumagai, M. Steam reforming of methanol over Cu/CeO_2 catalysts studied in comparison with Cu/ZnO and Cu/Zn(Al)O catalysts. *Top. Catal.* **2003**, *22*, 205–213. [CrossRef]
32. Avgouropoulos, G.; Ioannides, T. Selective CO oxidation over $CuO\text{-}CeO_2$ catalysts prepared via the urea-nitrate combustion method. *Appl. Catal. A Gen.* **2003**, *244*, 155–167. [CrossRef]
33. Tang, X.; Zhang, B.; Li, Y.; Xu, Y.; Xin, Q.; Shen, W. Carbon monoxide oxidation over CuO/CeO_2 catalysts. *Catal. Today* **2004**, *93–95*, 191–198. [CrossRef]
34. Zheng, X.; Zhang, X.; Wang, X.; Wang, S.; Wu, S. Preparation and characterization of CuO/CeO_2 catalysts and their applications in low-temperature CO oxidation. *Appl. Catal. A Gen.* **2005**, *295*, 142–149. [CrossRef]
35. Li, L.; Zhan, Y.; Zheng, Q.; Zheng, Y.; Lin, X.; Li, D.; Zhu, J. Water-Gas Shift Reaction Over Aluminum Promoted Cu/CeO_2 Nanocatalysts Characterized by XRD, BET, TPR and Cyclic Voltammetry (CV). *Catal. Lett.* **2007**, *118*, 91–97. [CrossRef]
36. Tonelli, F.; Gorriz, O.; Arrúa, L.; Abello, M.C. Methanol steam reforming over Cu/CeO_2 catalysts. Influence of zinc addition. *Quim. Nova* **2011**, *34*, 1334–1338. [CrossRef]